Numerical Simulation of Flow Through a Two-Strut Scramjet Inlet

Ajay Kumar*
NASA Langley Research Center, Hampton, Virginia

A three-dimensional, Reynolds-averaged Navier-Stokes code has been used to numerically analyze flow through a two-strut, supersonic combustion ramjet (scramjet) inlet configuration. It solves the governing equations in full conservation form using either a fully explicit or explicit-implicit method. An algebraic, two-layer eddy-viscosity model is used for turbulent flow calculations. The analysis allows inclusion of end effects that are caused by the aft placement of the cowl on the underside of the inlet. A special grid has been developed to accomodate the struts embedded in the inlet flowfield. Detailed numerical results are presented here for the two-strut configuration, and a comparison is made with the available experimental results.

Nomenclature

G	= inlet throat gap
H	= inlet height
M_1	= Mach number at inlet face
P	= pressure
P_1	= pressure at inlet face
T_1	= temperature at inlet face
u, v, w	= velocity components in x, y, z coordinates direction, respectively
W	= inlet width
x, y, z	= Cartesian coordinates
Λ	= sweep angle
δ_s	= sidewall compression angle
δ_s'	= strut leading-edge compression angle

Introduction

THE exponential growth of computer speed and storage capacity as well as algorithm sophistication has allowed the application of advanced numerical methods to practical design problems in many engineering disciplines such as fluid dynamics. More and more use is being made of numerical methods in analyzing complex flowfields than has been possible in the past. An important example is that of the inlet design of supersonic combustion ramjets (scramjets), where modern computational methods allow the direct numerical solution of the inlet flowfield in a reasonably efficient manner. The intelligent use of such capability can be very helpful in eliminating the poorer designs and allowing promising design configurations to be developed with less reliance on extensive wind-tunnel testing.

This paper discusses the application of a three-dimensional Navier-Stokes code to the analysis of high-speed inlet flowfields. NASA Langley Research Center has an ongoing research program to define and develop a viable air-breathing propulsion system for hypersonic flight application. In this flight regime, a supersonic combustion ramjet engine becomes attractive. The basic concept being developed uses a fixed-geometry, modular approach that integrates with the vehicle.[1,2] Figure 1 shows an engine module with a sidewall removed that served as an initial focus of research in scramjet technology at NASA Langley. The inlet of this module compresses the flow with swept, wedge-shaped sidewalls. The sweep of these sidewalls in combination with aft placement of the cowl on the underside of the engine allows for efficient spillage and good inlet characteristics over a range of operating Mach numbers with fixed geometry. The inlet compression is completed by three wedge-shaped struts (see the cross-sectional view in Fig. 1) that also provide locations for the injection of gaseous fuel. Considerable aerodynamic testing of this module has resulted in a baseline inlet design that performs well over a wide range of Mach numbers. The basic design features of this inlet are described in Ref. 3.

Because of possible diversified applications of scramjet engines, inlet research is now moving into investigating several new concepts that retain the basic features of the baseline design such as fixed geometry, sweep, struts, and cutback cowl. Most of this research has necessarily been experimental in the past due to the complex inlet geometries and the associated complex three-dimensional nature of the flowfield that does not lend itself to simple analytical estimates. However, with the increasing availability of supercomputers and advanced computing techniques, it is becoming more feasible to numerically calculate complex flowfields such as those associated with the high-speed inlets.

The effort to provide an inlet analysis tool started with the development of the two-dimensional Euler/Navier-Stokes code described in Ref. 4; this was followed by the fully three-dimensional Euler/Navier-Stokes code described in Ref. 5. These codes have already been used in the analysis of a variety of inlet configurations. The objective of the present paper is to further apply the three-dimensional Navier-Stokes code in simulating the flow through a new two-strut scramjet inlet design and to compare the numerical results with the available experimental data.

Outline of the Inlet Code

The code models the inlet flowfield using the three-dimensional Euler or Reynolds-averaged Navier-Stokes equations in conservation form. Those equations are transformed from the physical domain to a regular computational domain by using an algebraic numerical coordinate transformation that generates a set of boundary-fitted curvilinear coordinates.[6] The transformed equations are solved by either the explicit or explicit-implicit method developed by MacCormack.[7,8] In the case of turbulent flow calculations, an algebraic, two-layer, eddy viscosity model due to Baldwin and Lomax[9] is used.

The code is operational on the Control Data VPS 32 (a specially modified CYBER-200 series computer with a 16 million 64-bit word primary memory) vector processing computer system. It has been optimized to take maximum advantage of the vector processing capability of the computer system. To

Received Oct. 16, 1987; revision received Feb. 2, 1988.

*Head, Computational Methods Branch, High-Speed Aerodynamics Division. Associate Fellow AIAA.

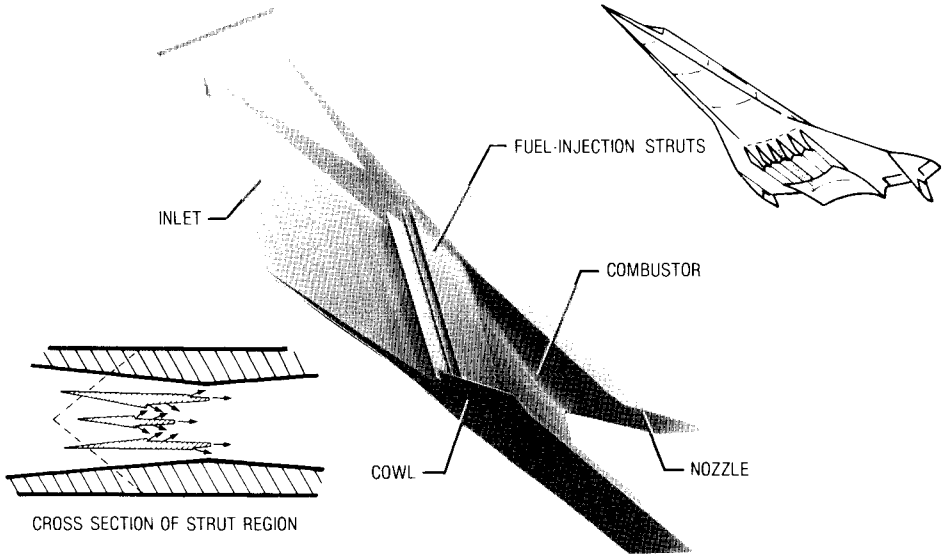

Fig. 1 A scramjet engine module and its cross section.

increase the number of grid points available for flowfield discretization, the code uses 32-bit word arithmetic. Working with 32- instead of 64-bit word arithmetic doubles the primary computer memory to 32 million words and reduces the execution time by a factor of little over 2 without adversely affecting the accuracy of the calculations. The maximum grid size that can be computed without going out of the primary memory of the computer is approximately 1.4 million points. The computing rate is about 0.7×10^{-5} s per grid point for one complete explicit time-step for the viscous flow calculations. More details about the code development and its organization are given in Ref. 5.

Boundary and Initial Conditions

The flow variables at the inflow boundary are held fixed at given freestream values, whereas extrapolation from the interior grid points is used to obtain the flow variables at the outflow boundary. No-slip and adiabatic-wall or known temperature conditions are used on the solid boundaries. The wall pressure is determined from the boundary condition that the normal derivative of pressure vanishes. On the open boundaries, extrapolation from interior grid points is used. If the flow is symmetric about a plane, only half of the flowfield is calculated and symmetry boundary conditions are imposed.

The boundary conditions are applied in both the predictor and corrector steps. Initial conditions are normally prescribed for each set of calculations by assuming that freestream conditions exist at all the grid points except at the boundaries where proper boundary conditions are applied.

Discussion of Results

The two-strut inlet configuration analyzed in this paper is shown in Fig. 2 with the cowl plate removed. A line diagram of the inlet is shown in Fig. 3. It has a rectangular cross section with swept wedge-shaped sidewalls and two swept compression struts located in the center passage. The sweep of all compression surfaces ends along line EF and cowl closure starts at F. The inlet model is parametric and allows adjustments in the overall geometric contraction ratio by moving the sidewalls and struts in and out. The cowl location can also be adjusted, and it is possible to add top surface compression, if desired.

In order to compare the numerical results with the experimental data, flow calculations for the preceding two-strut configuration are made at the following experimental conditions:

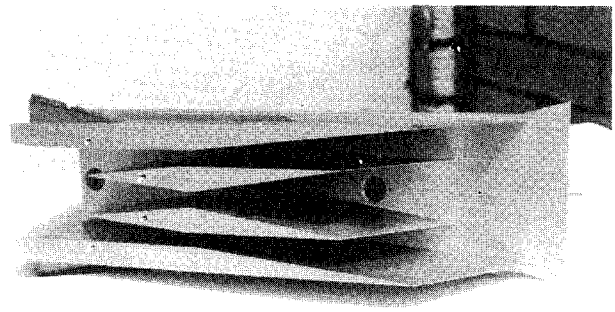

Fig. 2 Two-strut scramjet inlet configuration.

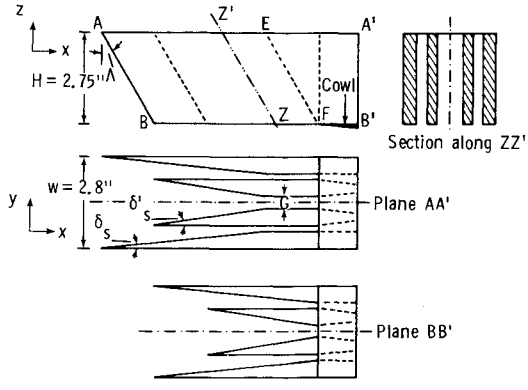

Fig. 3 Line diagram of the two-strut scramjet inlet configuration.

$$M_1 = 4.03$$
$$P_1 = 85{,}724 \text{ N/m}^2$$
$$T_1 = 70 \text{ K}$$

The inlet has a geometric contraction ratio W/G of 4.01 and zero top-surface compression. The cowl closure begins at the throat.

Before results of this calculation are presented, it is necessary to discuss how the present analysis includes the end effects in the inlet that arise from the interaction between the

internal and external flows. This interaction occurs because of the aft placement of the cowl that exposes the high-pressure internal flow to the low-pressure external flow in the region ahead of the cowl. The pressure differential causes an expansion wave to run into the inlet flow and a compression wave into the external flow, thus creating an induced flow in the downward direction ahead of the cowl. These end effects can significantly affect the inlet flowfield for certain flow conditions, and the induced flow set up by the end effects can result in substantial additional flow spillage other than that from the sweep of the compression surfaces. In order to account for the end effects in the analysis, a portion of the external flow under the plane of the cowl must be included. Ideally, one should go down and around the sidewalls far enough so that the free-stream conditions can be applied on the free boundaries, but this would greatly increase the computational requirements. In the present analysis, the region is extended as shown in Fig. 4 by the dashed line (only half of the inlet flow is calculated due to symmetry). This limited extension of the computational domain is found adequate so far as the inlet flowfield is concerned. Extrapolation from interior grid points is used all along the dashed-line boundaries except at the inflow boundary where the flow conditions are prescribed.

The calculations presented here are made with a grid of about 271,000 points (77 points in the x direction, 69 points in the y direction between the symmetry plane and sidewall, and 51 points in the z direction). Out of the 51 planes in the z direction, 14 planes are located under the cowl plane to account for the end effects. Discretization of this inlet is further complicated by the struts embedded in the flowfield. In order to accommodate the strut, the present analysis makes the strut surfaces coincident with two grid planes in the y direction and further allows 12 or more grid planes to go through the strut. This results in the slight blunting of the strut leading edge, but this blunting is relatively small due to grid refinement in the neighborhood of the strut surfaces. A typical grid in the symmetry plane and one of the cross planes is shown in Fig. 5. If a particular cross plane lies above the cowl plane, the grid points lying within the strut are neglected and proper boundary conditions are applied on the strut surfaces, but if the cross plane lies below the cowl plane, all grid points in the plane are used in the calculations. The preceding simplified approach in discretizing the inlet configuration, although it resulted in the waste of some grid points, avoided the need of using more involved grid-generation procedures.

Results of the present calculations are shown in Figs. 6–10. Figure 6 shows the velocity vector field and static pressure contours in a plane located at mid-inlet height. Although the calculations were performed only for half of the inlet, results are shown here for the full inlet by reflecting to the other half. The slight blunting of strut leading edges and associated small distortions in pressure contours in the immediate neighborhood of the strut leading edges are obvious from this figure. However, the impact of bluntness appears to be local. The velocity vector plot shows several regions of separated flow on the inlet surfaces caused by the shock/boundary-layer interactions and the pressure contour plot clearly illustrates the complex shock and expansion wave structure present in the inlet.

Figure 7 shows the velocity vector field and static-pressure contours in the symmetry plane of the inlet. The swept shock wave structure caused by the swept compression surfaces is obvious from this figure. The velocity vector plot shows significant flow separation near the top surface of the inlet caused by the shock/boundary-layer interaction. The velocity vector plot further shows a downturn in flow direction ahead of the cowl, resulting in some flow spillage from the inlet. This downturn is caused by the swept compression surfaces and the interaction in the cowl plane between the internal and external flow (the so-called end effects). Once the inlet flow passes behind the cowl leading edge, it is turned back parallel to the cowl plane; this turning results in a cowl shock that can be seen clearly in the pressure contour plot of Fig. 7.

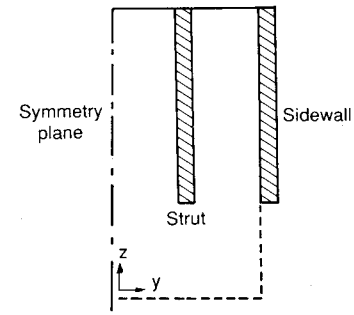

Fig. 4 Physical domain of computation.

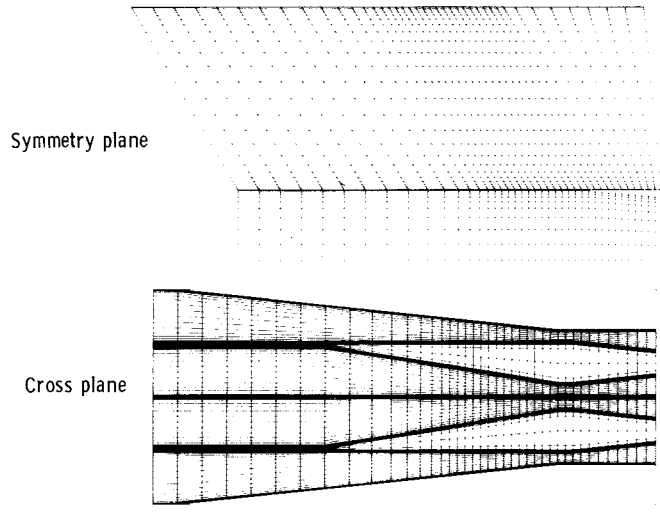

Fig. 5 Computational grid.

Figure 8 shows the sidewall pressure distributions at two inlet height locations. Experimental results from Ref. 10 are also shown. It is seen that the present results compare very well with the experiment at both height locations. Figure 9 shows the pressure distribution on the strut inner surface (i.e., the surface facing the symmetry plane) at the mid-inlet height location. Here again, a comparison with the experimental results of Ref. 10 shows very good agreement. The preceding good agreement with the experimental results is significant, considering the fact that the flow in the throat region of the inlet is highly complex due to the interactions of sidewall and strut shock and expansion waves, cowl shock, expansion waves due to the end effects, and induced shocks caused by the flow separation, all of which are taking place in relatively small gaps between the sidewalls and struts.

As mentioned earleir, not all the flow approaching the inlet face is captured by the inlet. Some of it is spilled out because of the swept compression surfaces and end effects. The amount of flow captured by the inlet is an important measure of inlet performance. Figure 10 shows a comparision of the predicted inlet capture with the experiment as a function of the axial distance from the inlet leading edge. It is seen that the predicted capture distribution agrees very well with the experiment.

Preceding good agreement with the experimental results shows that the inlet code has very well simulated the complex flowfield of the two-strut inlet configuration. The results also substantiate the adequacy of the procedure used in the analysis to include the end effects and to accommodate the embedded struts in the flowfield.

Concluding Remarks

A three-dimensional Navier–Stokes code has been used to analyze the complex flowfield through a two-strut scramjet in-

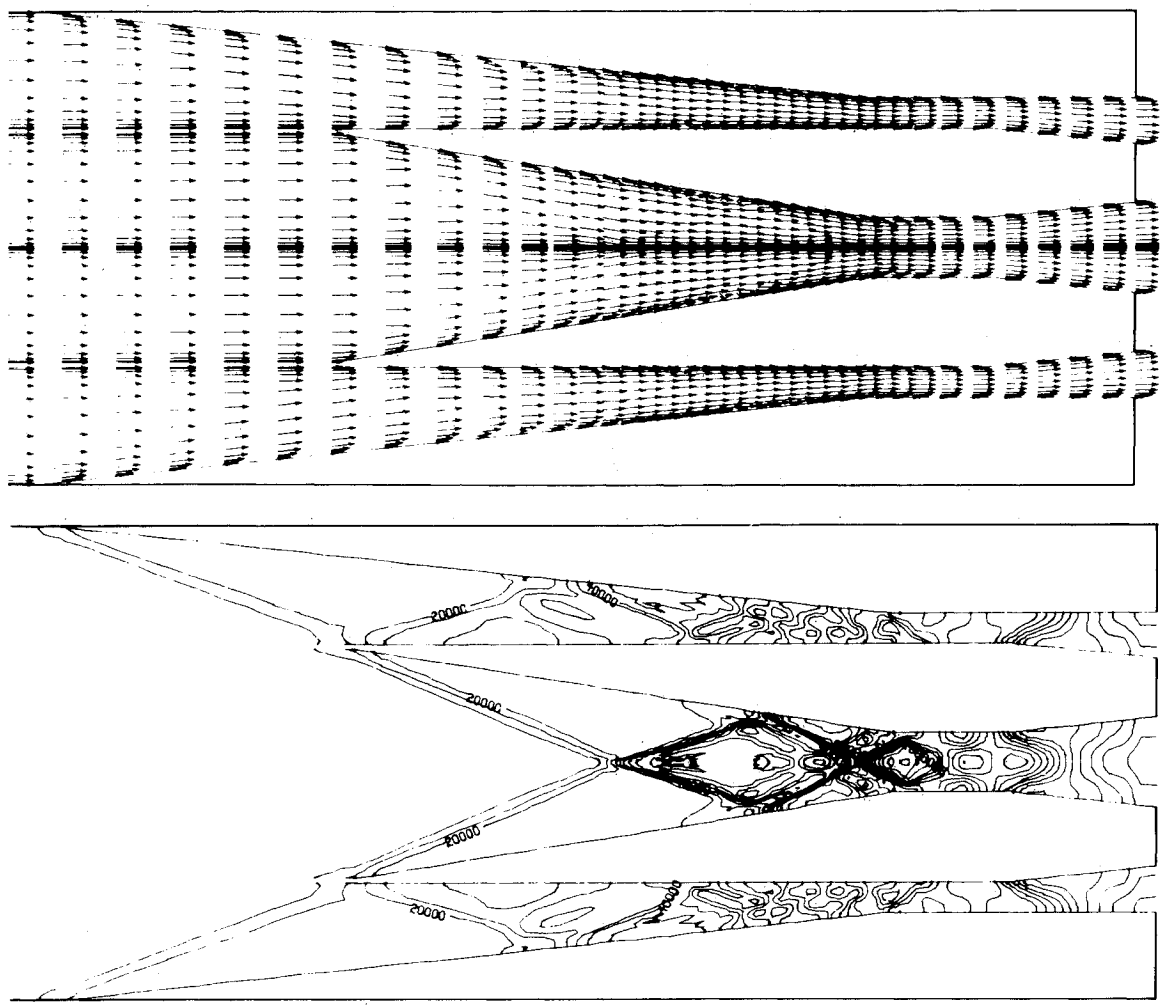

Fig. 6 Velocity vector field and pressure contours in a plane located at mid-inlet height.

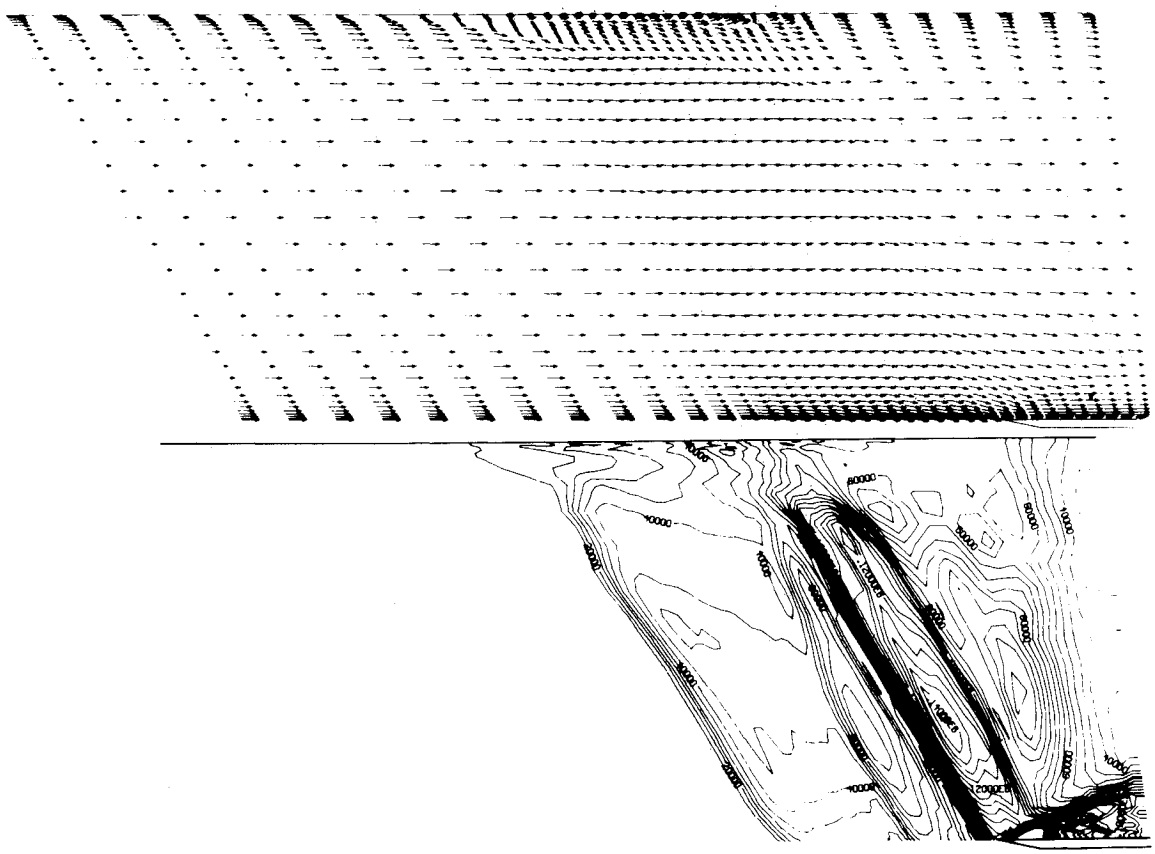

Fig. 7 Velocity vector field and pressure contours in the symmetry plane.

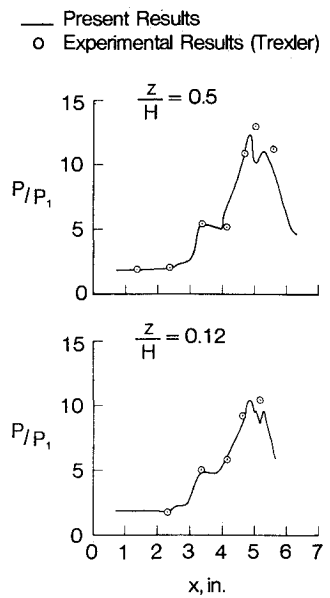

Fig. 8 Pressure distribution on the inlet sidewall.

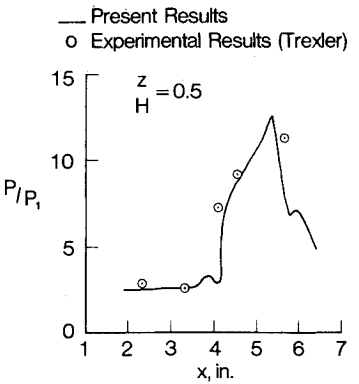

Fig. 9 Pressure distribution on the strut inner surface.

let configuration. The analysis allows inclusion of end effects that arise due to the aft placement of the cowl, resulting in interaction between the high-pressure internal flow and the low pressure external flow in the region ahead of the cowl. A special grid has been developed to accomodate the embedded struts in the inlet flowfield. The calculations are made using approximately 271,000 grid points in order to be able to properly resolve the viscous effects as well as the flow in the throat region of the inlet. The very good agreement of the present results with the available experimental results shows that the

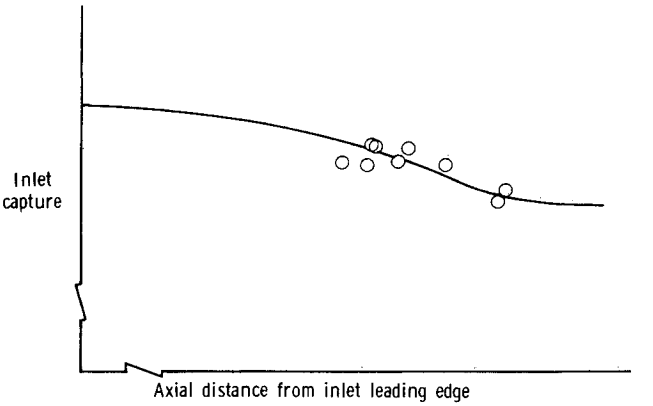

Fig. 10 Axial distribution of inlet capture.

inlet code has well simulated the complex flowfield of the two-strut inlet configuration.

Acknowledgment

The author would like to thank Carl A. Trexler of the Hypersonic Propulsion Branch at the NASA Langley Research Center for providing the details on the inlet configuration and the experimental results.

References

[1]Jones, R. A. and Huber, P. W., "Toward Scramjet Aircraft," *Astronautics and Aeronautics*, Vol. 16, Feb. 1978, pp. 38-49.

[2]Beach, H. L., Jr., "Hypersonic Propulsion," Paper XII, NASA CP-2092, May 1979.

[3]Trexler, C. A., "Design and Performance at a Local Mach Number of 6 of an Inlet for an Integrated Scramjet Concept," NASA TN D-7944, 1975.

[4]Kumar, A., "Numerical Analysis of the Scramjet Inlet Flow Field Using Two-Dimensional Navier-Stokes Equations," NASA TP-1940, 1981.

[5]Kumar, A., "Numerical Simulation of Scramjet Inlet Flow Fields," NASA TP-2517, 1986.

[6]Smith, R. E., "Two-Boundary Grid Generation for the Solution of the Three-Dimensional Compressible Navier-Stokes Equations," NASA TM-83123, 1981.

[7]MacCormack, R. W., "The Effect of Viscosity in Hypervelocity Impact Cratering," AIAA Paper 69-354, May 1969.

[8]MacCormack, R. W., "A Numerical Method for Solving the Equations of Compressible Viscous Flow," *AIAA Journal*, Vol. 20, Sept. 1982, pp. 1275-1281.

[9]Baldwin, B. S. and Lomax, H., "Thin Layer Approximation and Algebraic Model for Separated Tubulent Flows," AIAA Paper 78-0257, Jan. 1978.

[10]Trexler, C. A., "The Design and Performance at Mach 4.0 of Two-Strut Hypersonic Inlets for an Integrated Scramjet Concept," NASA TM 4022, 1988.